

EVALUATION OF A NEW APPROACH FOR THE INSPECTION OF AUSTENITIC DISSIMILAR WELDS USING ULTRASONIC PHASED ARRAY TECHNIQUES

Capucine CARPENTIER¹, Channa NAGESWARAN¹ and Yau Yau TSE²

¹ TWI Ltd, Granta Park, Great Abington, Cambridge, UK, CB21 6AL, 01223 899 000

² Metallurgy & Materials Dept, University of Birmingham, Edgbaston, UK, B15 2TT

Corresponding author: capucine.carpentier@twi.co.uk

1 Introduction

The fundamental obstacle to accurately characterising the defects in austenitic welds is the distortion of the sound field due to the anisotropic inhomogeneous material. This paper describes the development of the next generation of ultrasonic procedures which use phased array techniques and models to account for the distortion of the sound field, such that the detection, positioning and sizing of defects is improved in comparison to current capabilities.

Development of special transducers can improve signal-to-noise performance, hence detection capability. However to overcome the distortion and improve characterisation, the material condition has to be accounted for in inspection design. Electron back scatter diffraction (EBSD) techniques were used to evaluate the texture of the weld and then the microstructural information was input to a model capable of propagating ultrasonic waves through the anisotropic inhomogeneous medium. With knowledge of the distortion, a strategy was developed for improving inspection by adapting focal laws using time reversal concepts to improve sensitivity. This paper presents the methodology for the correction strategy and the demonstration of its performance. This project is funded by the UK Technology Strategy Board (www.dissimilarweld.co.uk) whose role is to promote and support research into, and development and exploitation of, technology and innovation for the benefit of UK business, in order to increase economic growth and improve the quality of life.

This paper follows the paper given in the 7th NDE conference in relation to nuclear and pressurised components (Yokohama, 2009), where the early development of the strategy for adapted law was presented [1]. The project is ongoing and this paper outlines the full development and the performance evaluation undertaken to date.

2 Microstructural quantification and lengthwise uniformity study

The weld specimen studied in this project represented a typical joint used for the safe-end in pressurised water reactors (PWRs). The specimen was an 85 mm thick dissimilar butt weld between ferritic steel (50D) and stainless steel (316L) plates. Cladding (309L/ 308L) was applied on the bottom of the ferritic plate. An InconelTM 182 buttering was deposited at the interface with the ferritic side. The weld material was InconelTM 82/182 filler and the weld was a manual arc process performed in down-hand position. The weld preparation and geometry is shown in Figure 1. Several flaws were implanted into the weld in different positions. In this paper only two, Flaw 1 and Flaw 3, are discussed (Figures 2 and 3).

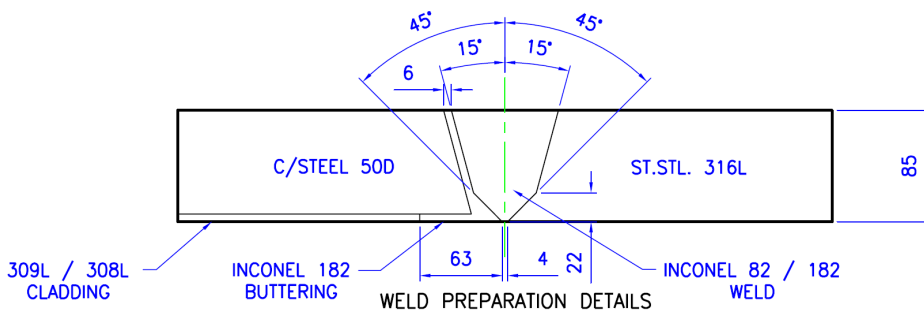


Figure 1 Weld specimen studied.

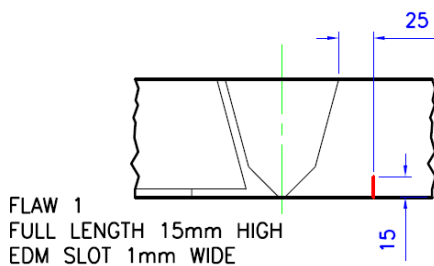


Figure 2 Detail of the Flaw 1.

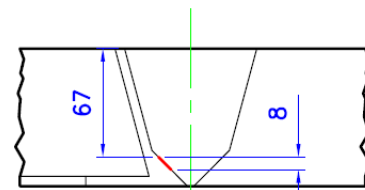


Figure 3 Detail of the Flaw 3.

Three samples were taken from a welded specimen for EBSD characterisation. EBSD is a powerful tool to perform crystallographic analysis of materials in a scanning electron microscope [2]. The orientation maps generated from EBSD contain quantitative information of the weld samples, such as crystallographic orientation, position of the grain boundaries and the grain sizes.

The EBSD generated the inverse pole figure map of the weld (Figure 4). This map provided the orientation of the crystallographic structure (face centered cubic) for each point of analysis taken every 40µm expressed with Euler angles and displayed over a gradient of orientation.

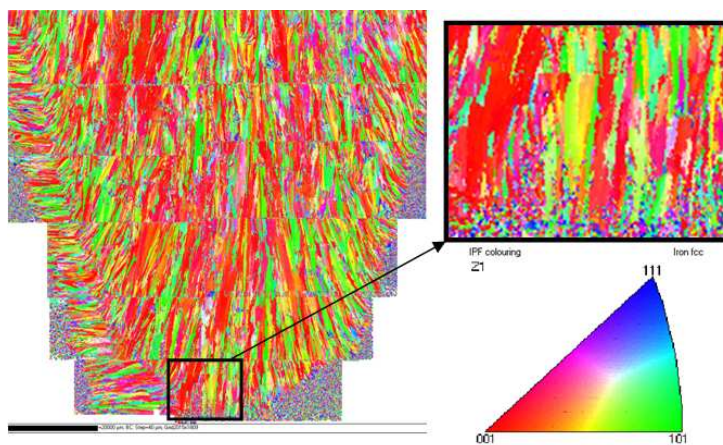


Figure 4 Inverse pole figure map of the front section taken in the weld specimen.

A post-treatment method was developed in order to identify the boundaries and the value of dominant orientations necessary for input into the wave propagation model. The Euler angles were translated into a different rotational angle coordinate system for the simulation program. Then, the grain boundaries were defined between areas of different orientation using a misorientation parameter for which the misorientation between two areas were greater than 20°. The crystallographic orientation in each of

these areas was defined using a grain unification factor for which the gradient of orientation smaller than 20° was unified to the major orientation. From this post-treatment, the orientation map was generated as shown in Figure 5.

The scanning resolution, the misorientation parameter and the unification factor were defined taking into account the Rayleigh scattering criterion [3]. This factor establishes the minimum dimension of the grain or area of dominant crystallographic orientation that interferes with the ultrasonic beam and generate beam scattering. The scattering phenomenon could become severe when the dimension of the grain approaches $\sim\lambda/10$ to $>\lambda$, where λ is the wavelength of the propagating sound wave. In the inspection of the weld specimen using 1.5MHz, scattering can occur for grain larger than $400\mu\text{m}$ to $4000\mu\text{m}$.

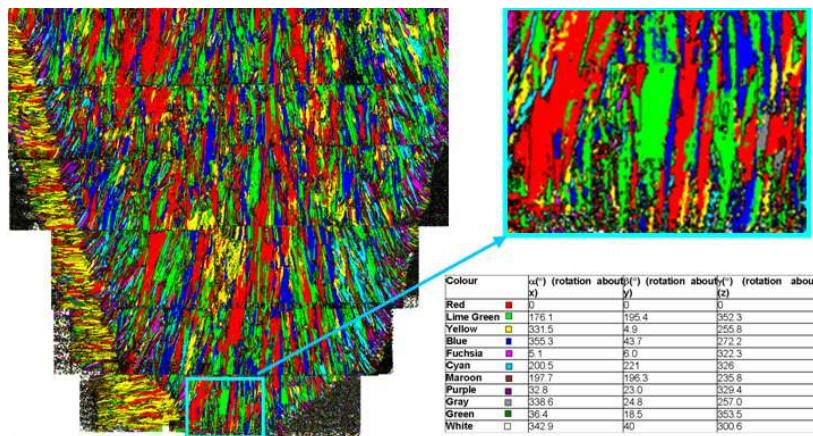


Figure 5 Unified orientation map of the front section taken in the weld specimen.

The three transversal sections were extracted from the front, middle and end part of the weld in order to evaluate the variation of the microstructure along the weld. Figure 6 shows the orientation map for each of these sections.

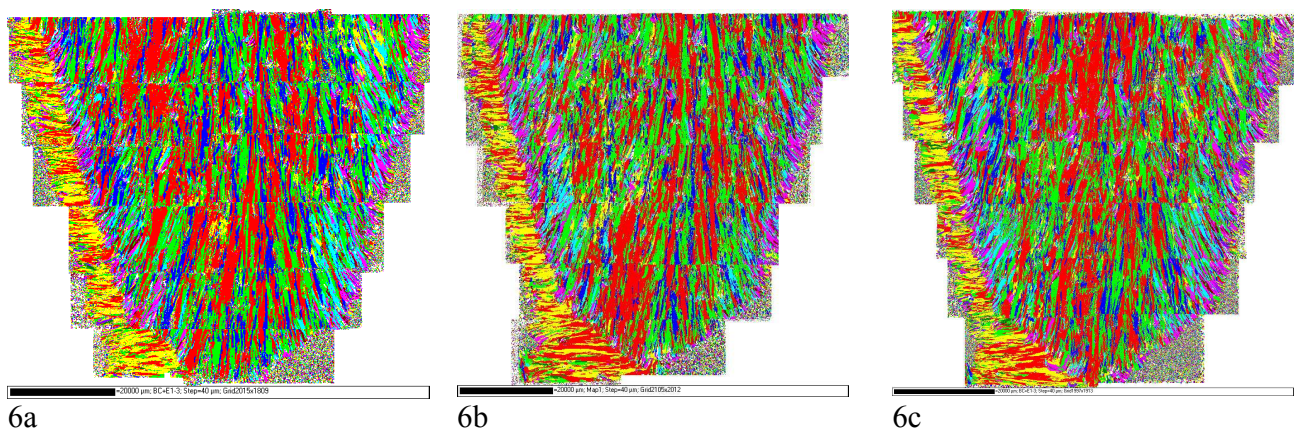
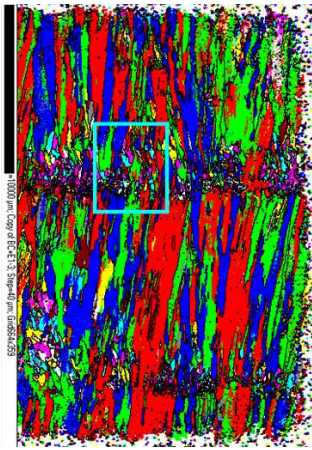


Figure 6 Orientation map of the transverse weld sections extracted from the weld specimen.
 6a Front section
 6b Middle section
 6c End section

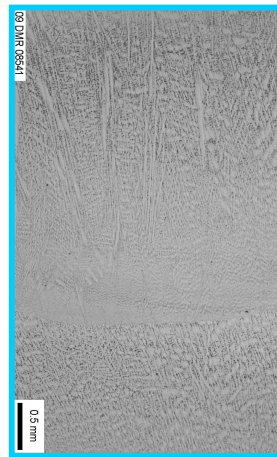
Longitudinal sections of the weld were also extracted as shown in Figure 7 in order to characterise the grains along the weld length. Samples L2 and L4 were scanned by EBSD and samples L1 and L3 were examined using optical microscope to observe the grain shape. Samples L2 and L3 were extracted near to the centre of the weld. Samples L1 and L4 were taken on the edge of the weld and near the buttering region. The EBSD orientation maps and macrographs are shown in Figures 8 and 9.



Figure 7 Positions of samples extracted from the weld for length measure of grains in y direction.



8a

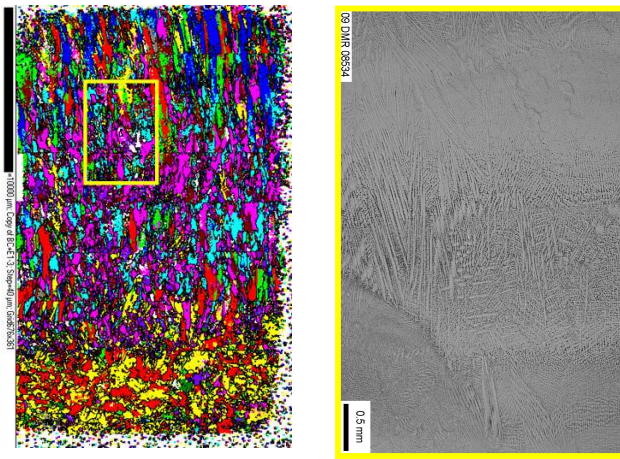


8b

Figure 8 Orientation map of the longitudinal weld sections extracted from the weld specimen in the centre of the weld (samples L2 and L3)

8a EBSD Orientation map of the sample L2

8b Macrograph from optical microscope of the sample L3



9a

9b

Figure 9 Orientation map of the longitudinal weld sections extracted from the weld specimen at the edge of the weld (samples L4 and L1)

9a EBSD Orientation map of the sample L4

9b Macrograph from optical microscope of the sample L1

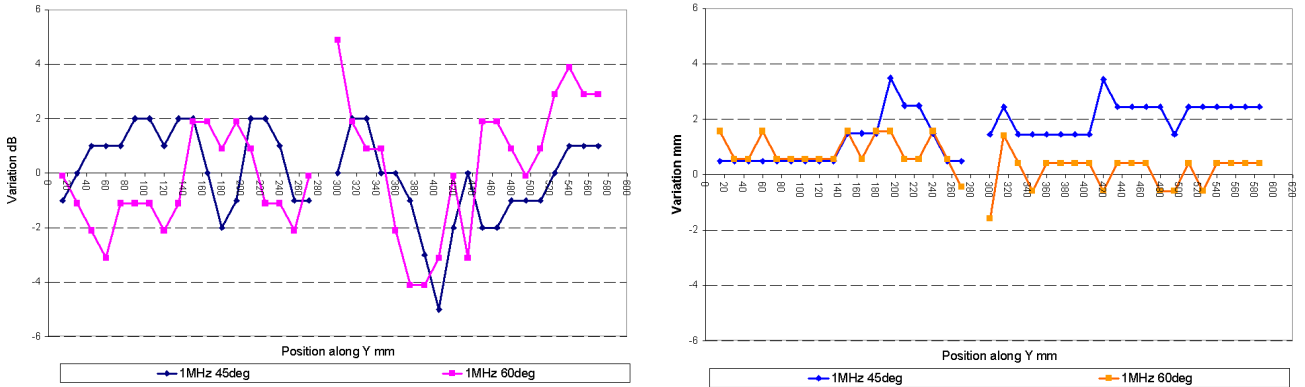
Analysis of the transverse sections of the weld suggests that the weld is defined by a characteristic columnar grain structure composed of eleven dominant crystallographic orientations expressed with different colors. The direction of these columnar grains is vertical in the weld body, horizontal in the buttering and tilted close to the weld fusion face. This arrangement is characteristic to austenitic and dissimilar welds [4]. It is the result of the partial melting between two weld beads where, during solidification, the resulting grain growth is defined by the heat flow and extends across several beads (epitaxial growth).

The comparison of the transverse maps at different positions along the weld shows that the dominant crystallographic orientations are conserved. However the distribution of these main orientations varied along the weld. Similar composition can be found at the start and the end of the weld. The longitudinal scans show that at the center of the weld the grains are also columnar and the crystallographic orientation is consistent with the transverse scan. At the edge of the weld the shape of the grains in this region are smaller and equiaxed. The average grain sizes were evaluated from the transverse and longitudinal orientation map and are listed in Table 1. Note that the average grain size of the largest grain is in the same order or larger than the ultrasonic wavelength used in the inspection (4000 μm). EBSD and optical micrograph results suggest that most of the orientated grains are rod-like in shape. The grains away from the edge of the weld are usually large and long and can interfere with the ultrasonic beam, whilst the grains near the edges are smaller, shorter and tilted.

	Transverse plane (XZ)		Longitudinal plane (YZ)	
	W (μm)	L (μm)	W(μm)	L(μm)
Buttering	Width of the butter	780 \pm 300	700 \pm 300	650 \pm 300
Large grains	900 \pm 300	10000 to 20000	648 \pm 200	10000 to 20000
Small grains	62 \pm 30	150 \pm 50	40 \pm 30	100 \pm 50

Table 1 Average grain size of columnar grains in different region of the weld.

In addition, the variation of the distortion along the weld was also investigated with ultrasonic measurements. The ultrasonic signal from a notch that runs the full length of the weld (Flaw 1) was monitored for a beam passing through the weld. Measurements were performed with two single crystal transducers 45 and 60°, both with a frequency of 1MHz. The amplitude of the signal and the vertical position of the slot corner were monitored along the weld. Figures 10a and 10b show, respectively, the variation of the signal amplitude and the variation of the vertical position of the slot corner with respect to the expected position (ΔZ).



10a

10b

Figure 10 Lengthwise uniformity along the weld measured with ultrasound

10a Amplitude of the ultrasonic signal coming from the slot corner (Flaw1)

10b ΔZ between the measured and the expected position of the slot corner (Flaw 1)

The signal amplitude fluctuates between ± 2 dB all along the weld. The ΔZ between the measured and the expected position of the slot corner also varied along the weld but the variation remains constant over a certain weld portion. The largest fluctuation is observed in the central part of the weld. There is good homogeneity in position along the weld when the beam passed through the weld body. The main effect of the anisotropy along the weld is on the variation in the signal amplitude.

Therefore, the results suggest that the quantification of the weld microstructure by EBSD for the definition through modeling of the correction factors to be applied during inspection may be done on few representative samples and be generic for similar geometries and welding procedures.

The quantitative information obtained was used to simulate the effect of grain orientations and boundaries on the ultrasonic beam propagation using a simulation platform [5]. Figure 11 shows the virtual map of the weld imported into the modeling platform. The weld structure was imported in 2D. The weld structure was assumed to be uniform along the welding direction. The elastic properties of each uniform orientation are defined by the elastic stiffness coefficient measured on a similar austenitic alloy to the weld studied using velocity measurements in a single-crystal. The measured stiffness constants are $C_{11}=203.6$ GPa, $C_{12}=133.5$ GPa and $C_{44}=129.8$ GPa [6].

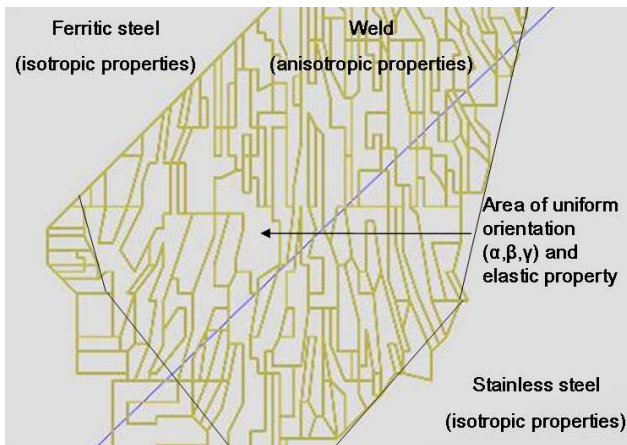


Figure 11 Virtual map of the front section of the weld specimen.

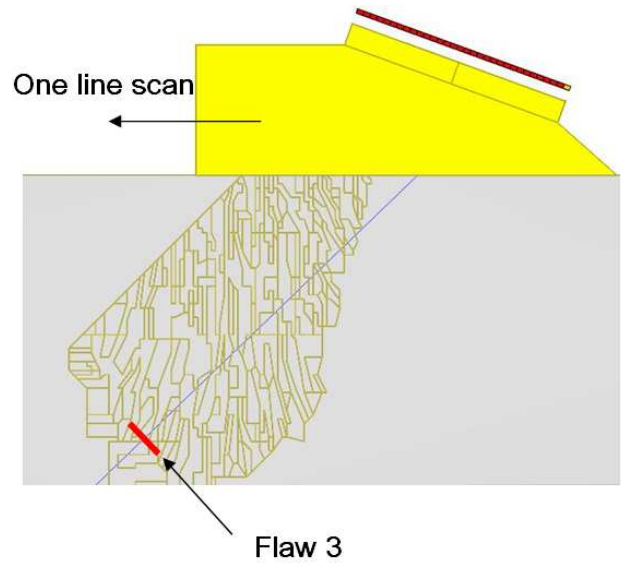
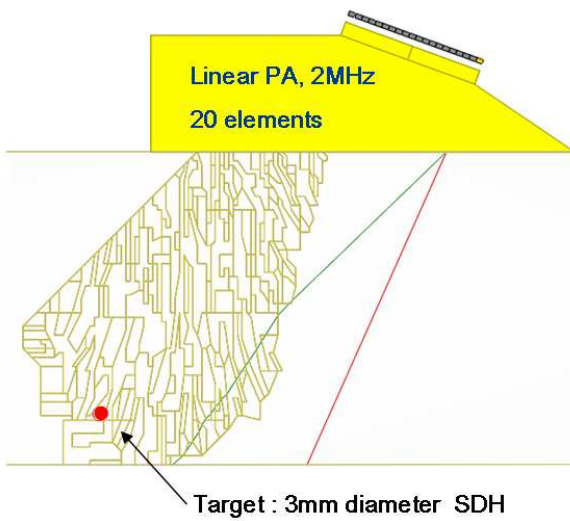
3 Correction Strategy

The anisotropic nature of the weld causes the velocity and the amplitude of the wave propagation to vary with direction. This behaviour has to be accounted for in order to compensate for the ultrasonic beam distortion and improve the reliability of the inspection.

Phased array techniques bring the capability to construct and control the sound field by using the principle of wave phasing. The phasing of each elementary wave is directed by the delays in transmission and reception that are applied to each element. These delays are calculated as a function of the time of flight of each elementary wave to reach the target in an isotropic media. In an anisotropic media, the wave phasing is distorted due to variation of the velocity in the path of the wave. This leads to defocusing of the ultrasound at the desired position.

The strategy developed in this project is to use modelling in order to predict the sound path for each element taking into account the anisotropic structure of the weld and adapt the delay laws. An analytical model of wave propagation (CIVA software developed by CEA, the French atomic commission) was used with input from the EBSD characterization in order to predict the effect of the anisotropy on the ultrasonic beam and generate adapted delay laws. The correction strategy is based on the time reversal method.

The concept of the correction strategy was demonstrated on Flaw 3 using a linear phased array transducer, 20° Perspex wedge, 20 elements and 2MHz frequency as shown in Figure 12. The adapted delay law was generated from signals of a 3mm diameter side drill hole (SDH) at the same depth as the flaw centre (Figure 12a).



12a

12b

Figure 12 Weld, transducer and target configuration used in the modeling for:

12a generating the adapted law (the green and the red lines are the ultrasonic ray tracing, longitudinal and shear wave mode, coming from the first element of the transducer).

12b scanning on the flaw.

The time of flight of the target's signal for each element were calculated. The delays applied on each of the transducer element were based on this time. Figure 13 shows the delay law calculated from the software for an ultrasonic beam steered at 46.5° in an isotropic media (stainless steel) and focused at the depth of the SDH. The shape of the isotropic delay law is a typical focusing delay law. The steering of the beam does not require phasing as the wedge angle generates a natural 46° beam in an isotropic media. Figure 14 shows the adapted delay law generated through modeling using the time reversal principal. The irregular shape of the adapted delay translates the effect of the weld anisotropy on the wave propagation.

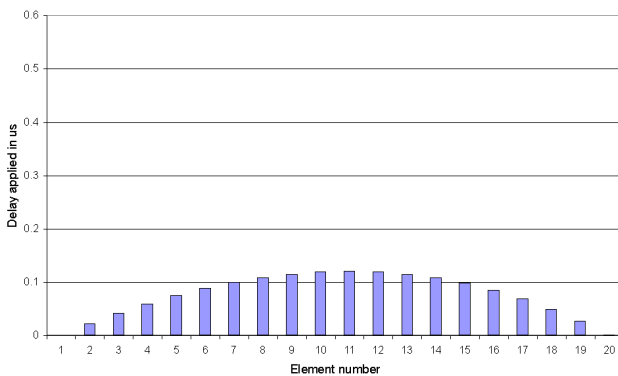


Figure 13 Isotropic delay law calculated.

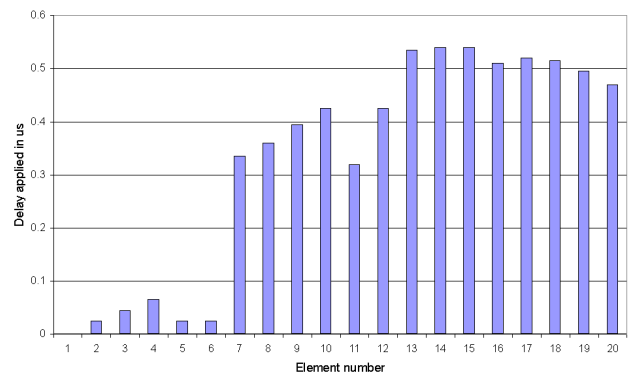


Figure 14 Adapted delay law generated with modelling.

As shown in Figure 12b, the transducer was then translated across the flaw. An A-scan was recorded every 2mm. Figure 15 shows the echo dynamic curves from the Flaw 3 due to the adapted delay law and the isotropic delay law, plotting the maximum amplitude of the A-scan at each position of the probe. Note that the centre of the flaw is in position zero.

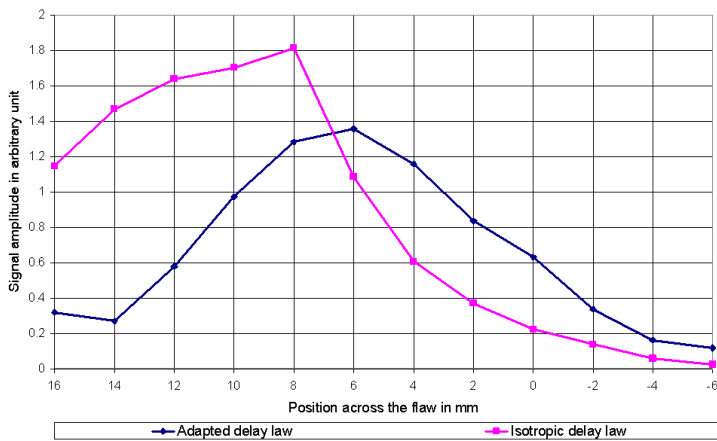


Figure 15 Modelling echo dynamic curves of the Flaw 3 with the adapted delay law and the isotropic delay law.

For both curves, the maximum amplitude reflected by the centre of the flaw is displayed outside the limit of the flaw. This is due to the beam skewing effect of the weld microstructure and the plotting of the data takes place without knowing the positioning error. Correction of positioning error is addressed using another technique (translation tables) [1].

The maximum amplitude with the adapted delay law is 2dB below that of the isotropic law. In the adapted delay law, there are six elements (elements 1 to 6) which are significantly offset from the remaining elements in time. The delays imply that the time of flight of elements 1 to 6 is significantly greater than the rest. Considering their position on the array and the path they take into the weld, it is unlikely that they are contributing to the main beam incident on the flaw, possibly explaining the reduction in received amplitude. The delay law curve of the remaining elements match well (both within $0.2\mu\text{s}$ between minimum and maximum delay) to the calculated isotropic law.

With the adapted delay law, the reflected amplitudes are distributed as expected for a specular flaw. In addition, the projected height of the flaw measured on this curve using the 6dB drop method (assuming that the ultrasonic beam is smaller than the flaw height) is 12mm which corresponds to the expected through wall height for the Flaw 3 (Figure 3). In comparison, the amplitude distribution is less uniform with the isotropic delay law. In this particular inspection case, the ultrasonic beam generated with the adapted delay law taking into account the weld microstructure appears to maintain integrity to aid flaw characterisation.

4 Performance demonstration

The concept of adapting laws was evaluated through experimental trials on the weld specimen on the Flaw 3 using the same phased array probe and wedge as in the modelling. A raster scan over the flaw was performed using the automated system called MIPS developed by British Energy. A 46.5° ultrasonic beam was generated using the adapted law produced through modelling (Figure 14) and the calculated isotropic law (Figure 13). Both signals were calibrated on 3mm diameter SDH at 70mm depth in a ferritic reference block. Amplitude of the signal across the flaw was recorded along a line scan in the middle of the flaw. Figure 16 shows the experimental echo dynamic curves of the Flaw 3 with the adapted and isotropic delay laws.

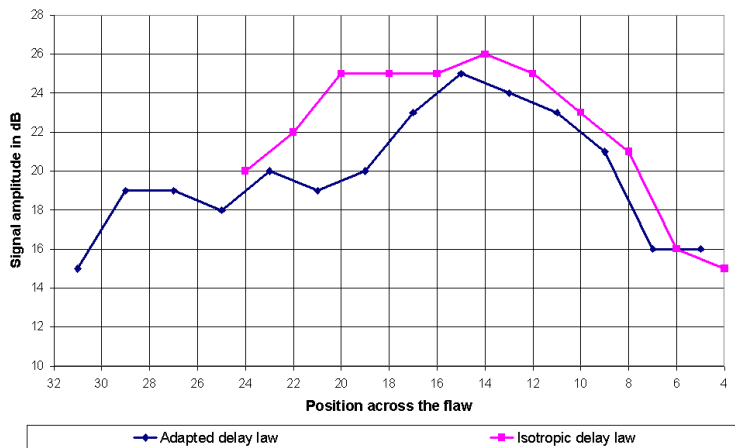


Figure 16 Experimental echo dynamic curves of the Flaw 3 with the adapted delay law and the isotropic delay law.

The reflected signal strength of the adapted delay law is less (1dB) than that using the isotropic delay law. There could be several reasons for this including the actual stiffness coefficients in the real weld not being the coefficients used in the model, which were obtained from literature, leading to an error in the adapted law. In addition, when the weld was mapped using the EBSD, thickness was lost due to the width of the saw. Hence the depth of Flaw 3 in the model was 58mm whereas in the component it was 70mm, with the result that the time of flights generated by the model not reflecting the actual scenario. With regard to the ultrasonic evidence shown in Figure 10, the variation in amplitude and positioning measured along the weld maybe significant enough to influence the adapted law in a particular weld section.

The width of the echo dynamic with the adapted law is smaller than with the isotropic flaw. The height of the flaw measured using the 6dB drop method is 13mm. It is possible that the local sound field generated due to the adapted law is more coherent, leading to lower distortion of the beam. This result corresponds to the output of the model. However, the accuracy of the experimental result cannot yet be validated until the actual size of the flaw is established through sectioning at the end of the project.

5 Conclusion

The evidence generated to date in this ongoing project shows potential for developing advanced ultrasonic procedures which will lead to increased confidence in specifying, manufacturing and operating austenitic welded components for the future generation of high temperature power plants. The following conclusions are drawn from the results presented in this paper:

1. EBSD technology allowed the quantification of the crystallographic texture of the weld (boundaries and orientation) needed in order to quantify the effect on the ultrasonic beam and correct for it.
2. The lengthwise uniformity study using both microstructure analysis and ultrasonic data showed that the microstructure does not vary significantly along its length. The dominant grain orientations are conserved over three sections and the impact on the signal amplitude and positioning (Flaw 1) is within acceptable limits. However, experimental evidence on inspection of Flaw 3 suggests that the adapted law is sensitive to the variation that does exist.

3. Simulation of the inspection of the Flaw 3 suggests that the ultrasonic beam generated with the adapted law is more coherent on the flaw leading to better sizing. This effect is also confirmed through experimental data. However, full evaluation is not possible until flaw sectioning.
4. Issues regarding differences between the modelled weld and the actual weld (stiffness coefficients, loss of thickness due to cutting and lengthwise microstructure variation) appear to make an impact on the experimental results, in particular the received amplitude.
5. The method being developed in this project is applicable to critical components due to the cost of implementation. The resources required in terms of replication and metallurgical analysis of welds, computing power and ultrasonic instrumentation are significant.

6 References

1. C Nageswaran, C Carpentier and Y Y Tse: 'Improving phased array ultrasonic testing using models to overcome austenitic weld distortion', Proc 7th Int Conf on NDE in Relation to Structural Integrity for Nuclear and Pressurised Components, Yokohama, May 2009.
2. Randle, V., 'Microtexture determination and its applications', London, Institute of Materials, 1992.
3. Papadakis, E P: 'Revised grain-scattering formulas and tables', J Acoust Soc Am, Vol 37 pp 703-710, 1965.
4. Gooch T G: 'Grain size and morphology in nickel-chromium alloy weld metal', TWI Member Report 405/1989, August 1989.
5. Mahaut S, Chatillon S, Leymarie N, Jenson F and Calmon P, 'Simulation tools for predicting non destructive testing of heterogeneous and anisotropic structures', Int. Conf on Ultrasonics, Vienna, 2007.
6. Lenkkeri J and Juva A: 'The effect of anisotropy on the propagation of ultrasonic waves in austenitic stainless steel', Reliability of Ultrasonic Inspection of Austenitic Materials, Belgium, 1980.

7 Acknowledgements

The authors would like to thank all members of the DISSIMILAR consortium (British Energy, Shell UK, HSE Nuclear Installations Inspectorate, Peak NDT, ALBA Ultrasound, Applied Inspection, Birmingham University and TWI) for their support and encouragement.